Neural Network Mapping and Clustering of Elastic Behavior From Tactile and Range Imaging for Virtualized Reality Applications

Ana-Maria Cretu, *Student Member, IEEE*, Pierre Payeur, *Member, IEEE*, and Emil M. Petriu, *Fellow, IEEE*

***Abstract*—To fully reach its potential, virtualized reality needs to go beyond the modeling of rigid bodies and introduce accurate representations of deformable objects. This paper explores neural networks and vision-based and tactile measurement strategies to investigate the intricate processes of acquisition and mapping of properties characterizing deformable objects. An original composite neural network framework is applied to guide the tactile probing by clustering measurements representing uniform elasticity regions and, therefore, direct sensors toward areas of elasticity transitions where higher sampling density is required. The network characterizes the relationship between surface deformation and forces that are exemplified in nonrigid bodies. Beyond serving as a planner for the acquisition of measurements, the proposed composite neural architecture allows the encoding of the complex force/deformation relationship without the need for sophisticated mathematical modeling tools. Experimental results prove the validity and the feasibility of the proposed approach.**

***Index Terms*—Deformable objects, elasticity modeling, neural networks, probing guidance, range imaging, tactile sensing.**

I. Introduction

CURRENT research in the area of deformable objects for virtualized reality is mainly focusing on the modeling of inherently elastic objects. Most research concerns itself with simulations and studies methods to respond to the computational cost of increasingly complex models and the requirements for a realistic interaction with deformable models. Such a realistic interaction places demanding constraints on processing times, particularly if haptic displays are involved. In response to the difficulties that are encountered in conducting strain–stress relationship measurements for objects that are made of materials that exhibit nonlinear behavior, the majority of applications leave the choice for the selection of elastic parameters to the user or choose some values for these parameters according to some *a priori* knowledge regarding the deformable object model. This represents an important limitation when an accurate material model is unavailable or when material properties are not known or are known with a low certainty. At best, an expert is asked to interact with an object and to provide feedback on the nature of deformation that the object exhibits. This is a subjective measure that can be satisfactory for certain types of applications but cannot be employed where accuracy is expected.

In those cases where measurements of elasticity are performed, often, a single probing of the object is used to elicit its elastic behavior. Although this can produce satisfactory results for objects that have homogeneous elasticity, it is unsuitable for objects that are nonhomogeneous and have varying elasticity in different parts of their body. Also, one single probing might result in incorrect results if the data collected for the single point are corrupted by noise. On the other hand, the procedure to collect elastic data from a large number of points is time consuming. These two aspects explain the considerable interest in finding fast sampling procedures for the measurement of the elastic properties of 3-D object surfaces. Appropriate sampling control algorithms should be able to minimize the number of sampling points by selecting only those points that are relevant to fully map the elastic characteristics.

There are four main categories of solutions that are encountered in the literature that gather the elastic behavior of objects—indentation [1]–[6], vibration-based measurements [7], sound-based measurements [8], [9], and vision-based measurements [10]–[13]. The most popular for daily engineering problems are indentation and vision-based measurements, whereas in medical applications, vibration and sound measurements are preferred due to the inaccessibility of measured organs.

This paper mainly addresses vision-based solutions to measure elasticity. The principle that is employed is the collection of a series of images before and after deformation is produced, individually analyzing the images, and extracting profiles to compute the deformation that gives a hint about the elastic properties of the objects. A pointwise correspondence is needed between the deformed and undeformed profiles to compute the deformation. Several methods have been proposed for this purpose. Markers can be directly mounted on the objects [11], [12], [14], or the correspondence can be established using speckle patterns [15], [16]. In the latter case, a thin-film coating is applied on the surface of the object to generate the necessary

Manuscript received November 15, 2006; revised January 29, 2008. This work was supported in part by the Communications and Information Technology Ontario Centre of Excellence, the Materials and Manufacturing Ontario Centre of Excellence, the Natural Sciences and Engineering Research Council of Canada, and the Ontario Graduate Scholarship Program.

A.-M. Cretu and P. Payeur are with School of Information Technology and Engineering, University of Ottawa, Ottawa, ON K1N 6N5, Canada (e-mail: acretu@site.uottawa.ca).

E. M. Petriu is with School of Information Technology and Engineering, University of Ottawa, Ottawa, ON K1N 6N5, Canada, and also with XYZ RGB, Inc., Ottawa, ON K2M 2A8, Canada.

Color versions of one or more of the figures in this paper are available online at http://ieeexplore.ieee.org.

Digital Object Identifier 10.1109/TIM.2008.919904

speckle and the change of patterns when the deformation of the object is observed.

Wang *et al.* [14] used a grid of markers that also serve as nodes in a finite-element method model. Using digital image processing (corner extraction), the coordinates of various feature points in the grid and their displacement are obtained. From this information, a strain field and the corresponding work-conjugate stress field are constructed, and the forces are computed by balancing the internal stresses at each node. A similar idea was exploited by Kamiyama *et al.* [11], [12]. A tactile sensor, which uses a transparent elastic body with markers, and a color charge-coupled device camera are employed to measure the elastic behavior of the objects. By taking images of a certain marker in the interior of an elastic body, the variation information of the interior is measured when a force is applied to the surface of an object that is considered homogeneous and with linear elasticity. The variation information of the interior is then used to reconstruct a force vector distribution. Vuskovic *et al.* [13] used a specially designed instrument to measure hyperelastic isotropic materials, such as living tissues. The measurement method, which is based on pipette tissue aspiration, consists of leaning a tube against the tissue and gradually reducing the pressure in the tube. As the organ remains fixed to the tube, there are well-defined boundary conditions, and a complete description of the deformation is given by the profile of the aspirated tissue. The measurements are done with a vision setup. An optical fiber illuminates the scene, and the deformation is captured by a camera via a small mirror that is placed beside the aspiration hole. From the pictures, the material parameters are determined using the inverse finite-element method. A Levenberg–Marquart parameter identification algorithm performs a minimization of the difference between the measured load-deformation data and the data obtained using the finite-element method [13].

Ferrier and Brockett [15] and Hristu *et al.* [16] described a deformable image-based tactile sensor consisting of a roughly elliptical membrane, which is filled with fluid-like gel and inscribed with a grid of dots at precisely computed locations of the inner surface of the membrane. A fiber-optic cable illuminates the interior surface, and images of the grid are taken as the membrane deforms. A solution for the 3-D coordinates of the grid is obtained based on the assumptions that the volume enclosed by the membrane remains constant, the boundary of the membrane is fixed, and the portion of the membrane that is not in contact will assume a shape that minimizes its elastic energy.

A neural-based solution without an explicit computation of elasticity is presented by Greminger and Nelson [10], who took images after and before deformation to train a back-propagation neural network that defines the deformation of an elastic object that is submitted to an external force. The inputs to the network are the coordinates of a point in an undeformed body and the applied load on the body, and the outputs are the coordinates of the same point in the deformed body. The training data pairs are directly obtained from images of the object under known loads, and therefore, the neural network model is created without an explicit computation of the elastic parameters. A computer vision deformable body tracking algorithm based on a boundary-element method is applied to measure the displacement of a point in the undeformed body.

The majority of these methods make the assumption that the material exhibits linear elastic behavior and that the objects are homogeneous from the elasticity point of view or make use of another method (e.g., a finite-element method and a boundary-element method) to recoup the elasticity information and/or model the object. In this paper, an approach is investigated to develop a model that is not specific for a certain application but provides a representation for different objects to be introduced in virtualized reality environments.

The proposed modeling scheme that is presented in this paper is an extension of our previous work in this research area [17], [18] and leads to a model that is stand-alone and does not imply the use of heavy mathematical deformable object representation techniques. Also, the neural architecture that is considered provides guidance toward the sampling points that are the most relevant for the elastic behavior of an object. This provides a critical advantage by allowing to model at the same time objects that have nonlinear elasticity and that can also be nonhomogeneous from the elasticity point of view. The modeling of the elastic behavior is based on a separate neural network that stores the elasticity information without the need to explicitly recoup elastic parameters. As a major addition to our previous modeling scheme [18], the process of elastic behavior characterization is improved by the addition of supplementary inputs to the neural network that represent different angles of interacting forces.

II. Proposed Modeling Scheme

The proposed modeling framework advantageously combines various neural network architectures to achieve diversified tasks as required for data collection and modeling of elastic characteristics. During the first phase, a nonuniform adaptive sampling algorithm based on a self-organizing neural architecture is implemented to selectively collect data only on those points that are relevant for mapping the elastic behavior of an object. Starting from a 3-D cloud of points collected on an object or a scene of objects via an active range sensor, a neural gas network obtains a compressed model for the data set in which the weight vector consists of the 3-D coordinates of the objects' points. During the learning procedure, the model asymptotically contracts toward the points in the input space, with reference to their density and, thus, taking the shape of the objects that are encoded in the point cloud. These modeling properties ensure that the density of the tactile probing points is higher in the regions with more pronounced variations in the geometric shape. The advantage of such a model is not only to identify relevant sampling points but also to allow for the determination of clusters of sampling points with similar geometric properties due to its ability to find an optimal finite set that quantizes the given input space. This provides a robust mechanism that can be extended to model nonhomogeneous objects as well. The neural gas architecture, implementation, and use for adaptive sampling are detailed in [17]. Neural gas is selected instead of other self-organizing architectures after several experimental tests due to its accuracy, which is proved by

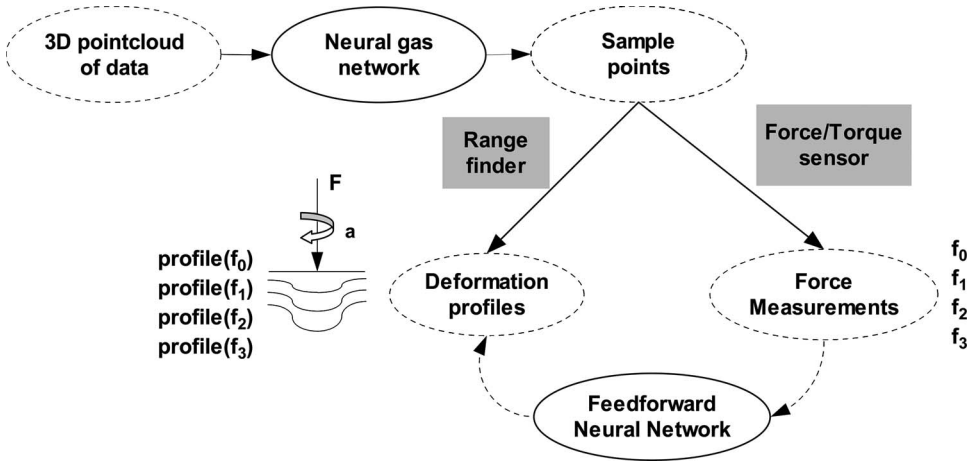

Fig. 1. Structure of the proposed neural-based sensing and mapping framework.

small distortion errors and its ability to capture fine details, as opposed to other architectures that obtain larger distortions and tend to smooth fine details, such as the Kohonen self-organizing map (SOM). An extended comparison between neural gas and the SOM in the context of adaptive sampling can be found in [17]. Even if the training procedure is longer in comparison with the SOM, we chose neural gas because the main goal in the context of this paper is the accuracy of models, as opposed to the real-time behavior of simplified computer-generated and simulated models, which has already been extensively studied in the literature.

Another neural architecture, i.e., a feedforward neural network, is employed to model the force/deformation behavior of selected sample points that are simultaneously probed by a force/torque sensor and a linescan active range sensor. Such an approach not only allows the recovery of the elastic parameters in the sampled points but also provides an estimate of the elastic behavior of surrounding points that are not part of the selected sampling point set but are covered in the linescan profile that is collected by the laser range sensor. Fig. 1 illustrates the structure of the proposed approach.

Using this selective data collection scheme, an advantage is taken of the quantization properties of neural gas networks to split objects into clusters, therefore ensuring that different regions of possibly nonhomogeneous objects are distinctly treated. Each cluster is sampled more than once under the control of the selective sampling algorithm to ensure enough data for an accurate representation of elasticity. This approach also copes with possible noise and errors that are induced by the measurement equipment.

III. Force/Deformation Acquisition Setup

Given the fact that elastic constants are material-related parameters and do not accurately describe real-world objects in general, we do not attempt to explicitly recover elastic constants, nor stress or strain tensors, for an object under loading. Instead, quantities of interest are those that can be observed on the surface of an object, namely the deformation of the surface as the object is loaded by a measured external force at a given point [19].

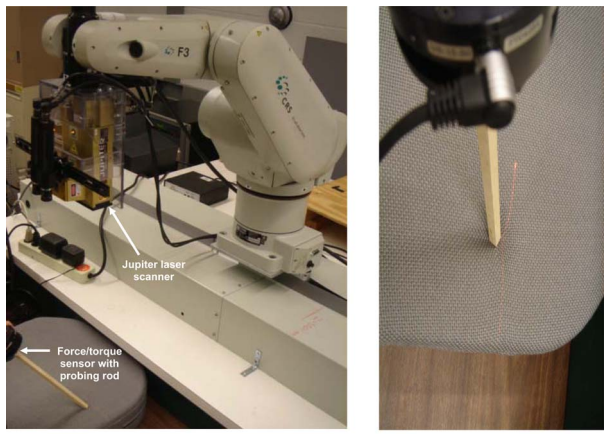

Fig. 2. (a) Range sensor and force/torque setup producing (b) laser trace to capture the object deformation resulting from the applied force.

The experimental setup that is used to collect force/deformation data is composed of a multiaxis *ATI* force/torque sensor [20], which is attached to a console computer, and an active triangulation line-scanning *Jupiter* laser range sensor [21], which is controlled via a second PC system, as depicted in Fig. 2(a). The force/torque sensor is used to record the force components that are applied on the object, whereas the range finder captures the deformation of the surface of an object under a given load. Fig. 2(b) illustrates the force/deformation data collection procedure on a deformable object representing one uniform cluster. The range finder is positioned such that the scanline intersects with the point where the external force is applied, as highlighted by the trace of the laser on the object.

The raw deformation profiles are encoded under the form of a 2-D distribution of points in the $Y-Z$ space, as shown in Fig. 3, where Y is the lateral displacement along the scanline, and Z is the depth along the optical axis with respect to a back-reference plane. The laser range finder provides a fast scan of 256 samples that are distributed along the straight scanline on the surface; 30–50 scans of the same area are collected within a few seconds, whereas the applied force and angle are kept constant. This provides efficient means to cope with the noise in the range data. Moreover, with the success of the range

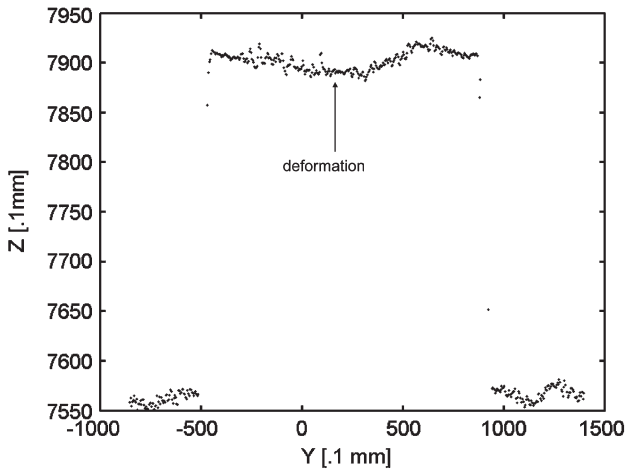

Fig. 3. Deformation profile mapped in the $Y-Z$ space.

data collection being highly sensitive to the texture and the orientation of surfaces, missing measurements usually appear along the scanline. The use of an iterative sampling procedure over a short period of time partially alleviates the impact of this constraint.

To filter out the average noise and include as many valid measurements as possible in areas where points can be missing in some of the scans, the mean value is computed on the depth (z-axis) over all the deformation profiles obtained under a given force from the sampling points belonging to each cluster. The resulting profiles are then saved for each magnitude and angle of force that are applied on the object and for each cluster of similar elasticity.

The use of range profiles rather than full intensity images eases up the training procedure of the neural network, as only significant deformation features are retained. The dimensionality of the vision data set is reduced to a vector indexing depth (Z) measurements along the scanline, which can be directly fed into the neural network.

IV. Neural Network Modeling of the Elastic Behavior

Given the nature of the modeling framework, there is no need to recoup the explicit deformation information from the range profiles. Instead, a neural network is used to learn the elastic behavior as a complex function of the force and the corresponding deformation profile. One network is used to model the elastic behavior of each material (cluster). The proposed neural architecture models the raw range data that are mapped in the $Y-Z$ space as a function of the applied force F. For each cluster of similar elasticity, a feedforward neural network with two input neurons that are associated with the magnitude and the angle of the applied force (F, a), 45 hidden neurons (H_1-H_{45}), and an output vector with the same size as the length of the deformation profile Z, as shown in Fig. 4, is employed to learn the relation between forces and angles and the corresponding deformation profiles provided by the range finder. From the several tests performed, 45 hidden neurons gave a good compromise between the accuracy of modeling and the length of training. The pointwise correspondence that is required between the deformed and undeformed range profiles is ensured by the fixed position of the range sensor and of the objects during the data collection. Therefore, the parameter Y covers the same range for all measurements on an object (and material) during the acquisition and is not considered to be an input in the network, with the Z values being uniformly indexed to the data vector.

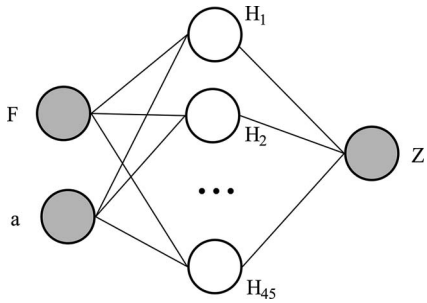

Fig. 4. Feedforward neural network to learn the elastic behavior from deformation profiles under various force magnitudes and angles.

Forces of different magnitudes that are applied at different angles from the tangent to the surface, which are not considered in our previous work due to experimental constraints [18], are now added as supplementary inputs in the network. This improves the modeled behavior, particularly for objects that are exhibiting highly nonlinear characteristics. Different magnitudes of forces at different angles are successively applied on the selected sampling points using the probe that is attached on the *ATI* force/torque sensor, and a series of overlapping profiles are collected with the laser range finder for each force magnitude before being averaged to reduce noise. The force magnitude F is computed as the norm of the three orthogonal force components along the x-, y-, and z-axes of the force/torque sensor's reference frame, as recorded by the device, i.e.,

$$F = \sqrt{F_x^2 + F_y^2 + F_z^2}.$$

The angle measurements are collected with the probe that is positioned in the plane parallel to the scanline that contains the probe tip, with the angle 0° starting on the far left and continuing up to the angle 180° on the far right, as depicted in Fig. 5. The normal force on the object's surface is considered at 90° with the tangent to the surface at the contact point.

Although the data are noisy and contain important gaps for large forces, the networks are directly trained with the averaged range profiles, as described in Section III, to avoid losing essential information. The only data preprocessing applied is a normalization of the depth data that are contained in the deformation profiles to the [0, 1] interval prior to training, as required by the neural network implementation.

For the training, several back-propagation algorithm variations were tested, namely the Levenberg–Marquart method, the quasi-Newton Broyden–Fletcher–Goldfarb–Shanno (BFGS) method [22], [23], and the resilient propagation (Rprop) [24]. The Levenberg–Marquart and quasi-Newton BFGS methods are classical gradient descent (steepest descent) methods, which are both variations of Newton's method. They use the gradient

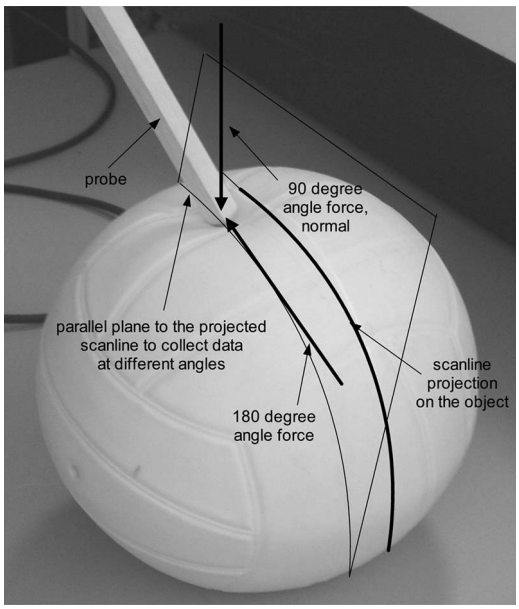

Fig. 5. Force measurement with different angles to the surface.

of the error function to compute the search direction (the negative gradient direction points to the locally steepest direction). The error function is considered to be quadratic, and, therefore, the direction toward the minimum error is determined by the inverse of the Hessian multiplied by the gradient, which is a product that is known as the Newton step. When the error function is indeed quadratic, Newton's method will find the minimum in one step, and if it is not quadratic, in most cases, it will quickly converge since many analytic functions can be accurately approximated in a small neighborhood of a strong minimum by a quadratic function. However, the exact computation of the inverse of the Hessian is computationally demanding. Furthermore, when the Hessian is not positively definite, the Newton step will move toward a maximum and not a minimum. The Levenberg–Marquart modification adds a term to the Hessian to ensure that it is always positive definite. To save the computation of the inverse of the Hessian, the BFGS method uses an approximation of it. Still, it is computationally demanding, and in those cases when the magnitude of the input is large, the derivative of the error function becomes very small, and all the steepest descent methods produce very small steps, sometimes never converging. In the present application, neither the Levenberg–Marquart method nor the quasi-Newton BFGS method succeeded in correctly capturing the characteristics of the deformation profiles. Due to the heavy memory loading implied, they were not able to model the entire deformation profile. Although it was possible to model a compressed version of the deformation profile, which is obtained by the replacement of each three sampling points by their average value, this solution was revealed to be insufficient to capture the fine details in the profiles. The resilient propagation method gives better results in significantly less time. In this method, the step size is not a function of the magnitude of the gradient, but rather depends on the sign of the derivative. If the sign of the derivative for a given weight remains the same over several iterations, then the magnitude of the step size is increased, and if the sign oscillates, the magnitude of the step size is decreased. The fact that only the sign of the derivative is used leads to an efficient computation with respect to time and storage consumption [24], even over long sets of deformation profiles with relatively smooth features.

Once trained, the network takes as inputs the force magnitude F and its corresponding angle of application a with respect to the tangent to the surface and takes as outputs the corresponding deformation profile as an indexed vector of depth values Z along the scanline.

V. Experimental Results

To validate the proposed modeling framework, experimentation was conducted on numerous deformable objects, of which a representative subset is reproduced here, i.e., a rubber ball and a simple composite object that is made of a square cardboard box mounted on the top of a covered foam pillow, as depicted in Fig. 6. This set of relevant examples is chosen, as it represents a significant combination of elastic materials, geometry, and texture properties that are all critical factors that influence the performance of the proposed approach. From the geometry perspective, we have rounded surfaces (a ball), edgy surfaces (a cardboard box), and combinations of both (a pillow with rounded edges), whereas from the elasticity perspective, we have a stiff material (cardboard), a semisoft material (rubber), and a highly nonlinear soft material (foam). Furthermore, some objects have a light color (the rubber is yellow, whereas the cardboard is light blue), whereas others have a dark color (the pillow is gray with a highly scattered texture). All those parameters influence the accuracy of measurements that are collected with the laser scanner, as explained further. The soft dark pillow is the most complex to be measured and modeled due to its nonlinear elastic behavior and nonuniform texture, which make the measurement using the laser range scanner difficult. Therefore, this example is shown to demonstrate the capability of the proposed method to cope with challenging modeling situations.

From the 3-D point cloud corresponding to the objects of interest, which is initially obtained with a complete scan of their entire surface with the laser range sensor, the adaptive sampling neural gas network returns a set of significant sampling points, as shown in Fig. 7(a) and (b) for the two objects under study. Points that are located along the contours of each element of the composite object are automatically highlighted, thus providing immediate target areas for tactile probing with the force/torque sensor.

In this experimentation, the fact that we consider a composite object with different elastic characteristics helps to study the case of objects with nonhomogeneous/piecewise homogeneous elastic behavior. The selected sampling points are clustered in two groups for the composite object, corresponding to the two deformable materials. In Fig. 7(b), the small points belong to the box, whereas the large ones belong to the pillow. Force/deformation data are then collected for each of them, using the setup described in Section III. A set of five measurements is collected with increasing force magnitudes at each of the 10°, 25°, 45°, 75°, 90°, 105°, 135°, 155°, and 170° angles.

Fig. 6. Deformable objects used for experimentation. (a) Rubber ball. (b) Composite object.

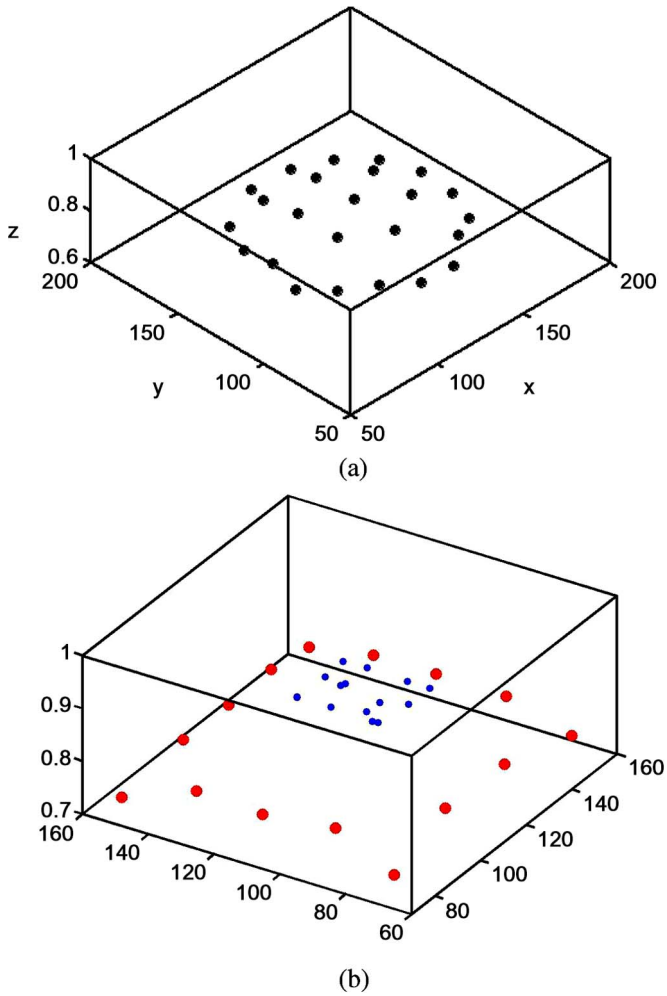

Fig. 7. Sampling points selected with the neural gas network for (a) a rubber ball and (b) a composite object.

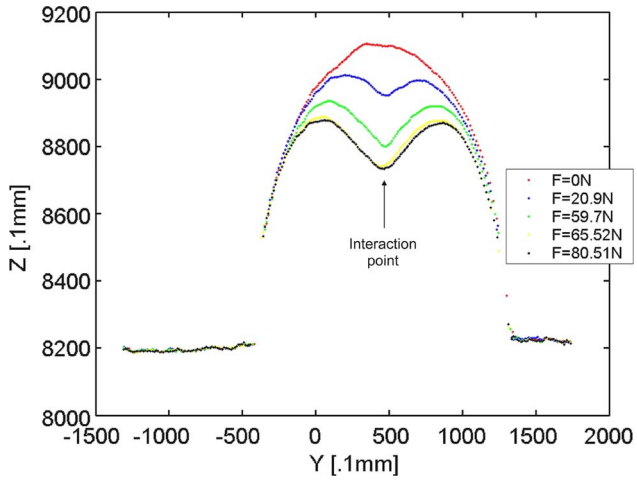

Fig. 8. Deformation profiles for the rubber ball under increasing normal force.

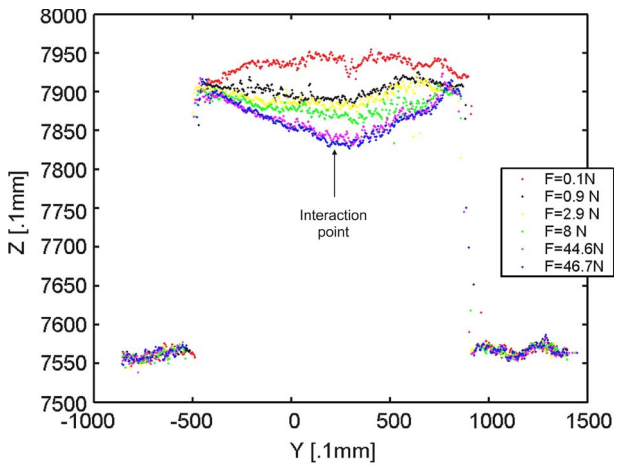

Fig. 9. Deformation profiles for the cardboard box under increasing normal force.

Figs. 8–10 show three examples of averaged deformation profiles resulting from the application of increasing forces along the normal direction to the surface of the object for the different materials under study. Figs. 11 and 12 show examples of averaged deformation profiles for the rubber and foam materials subject to different forces that are applied at different angles. The deformation profiles that are collected for angles under 90° present a deeper cavity around the probe's tip toward the right side, whereas the ones for angles that are larger than 90° have the cavity deeper toward the left side. As expected, angles that are closer to the normal to the surface usually lead to deeper deformation profiles, whereas tangential angles to the surface result in flatter profiles.

The quality of the collected range data is directly related to the material under study. As seen in Figs. 8–12, the range sensor data are more compact and less noisy for the rubber, which has a light color and a dense smooth texture. It is relatively compact for the cardboard, whereas measurements get scattered on a wider range of values and exhibit a larger number of gaps in the case of the foam. This effect is mainly due to the

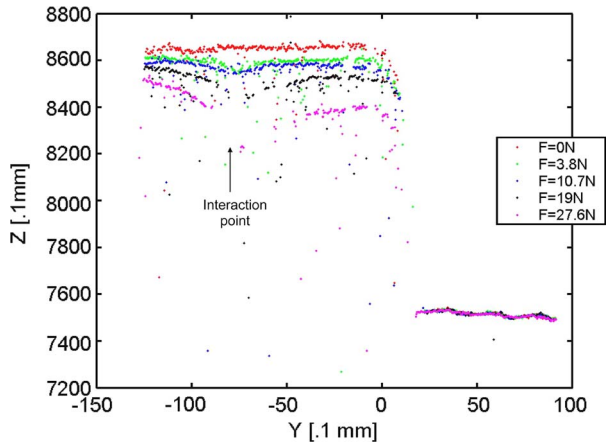

Fig. 10. Deformation profiles for the foam pillow under increasing normal force.

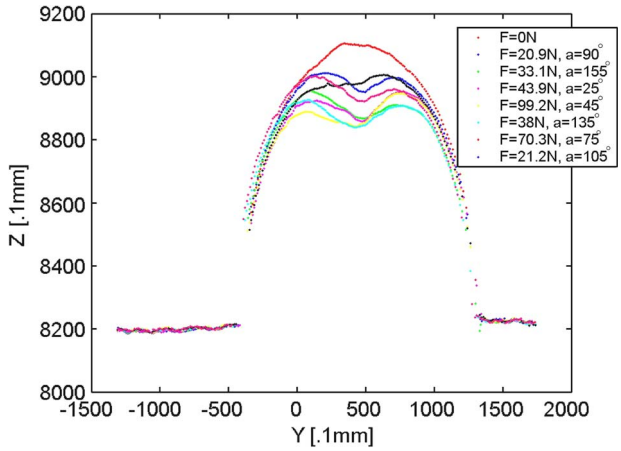

Fig. 11. Deformation profiles of the rubber ball under different magnitudes of the force applied at different angles.

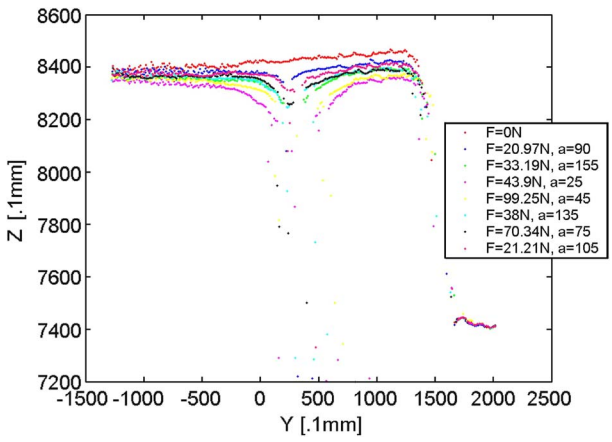

Fig. 12. Deformation profiles of the foam pillow under different magnitudes of the force applied at different angles (angles in degrees).

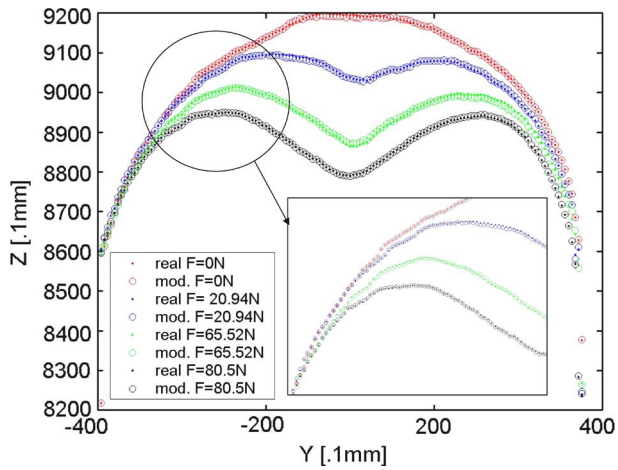

Fig. 13. Real and modeled deformation profiles and detail of the deformation for a rubber ball under normal forces.

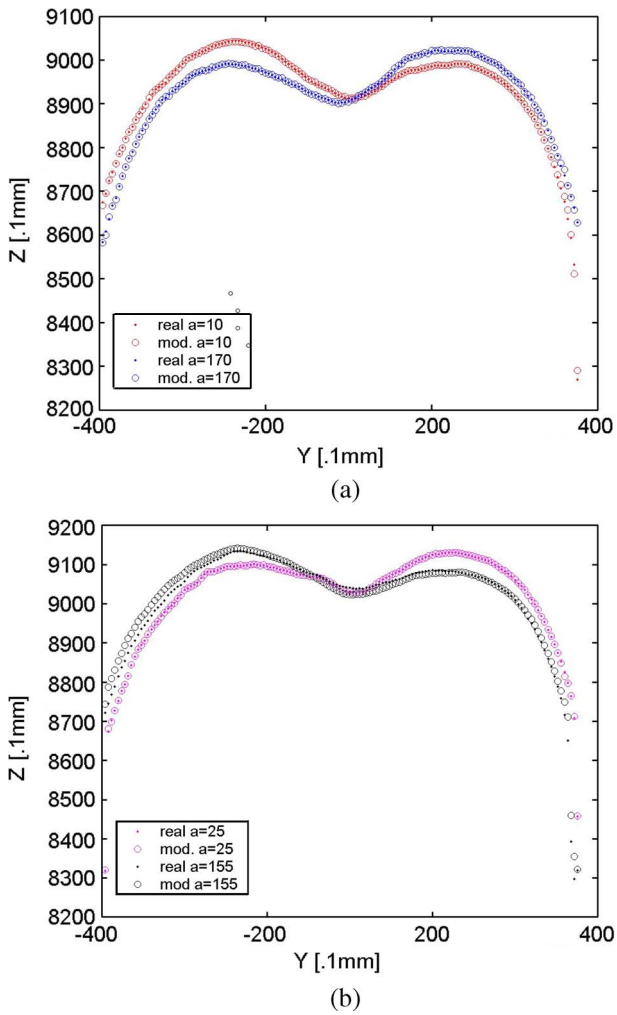

Fig. 14. Real and modeled deformation for a rubber ball under forces applied at different angles. (a) $F = 65$ N, $a = 10°$, and $F = 65$ N, $a = 170°$. (b) $F = 36$ N, $a = 25°$, and $F = 36$ N, $a = 155°$.

rough dark texture of the fabric that covers the piece of foam. As the laser range finder operates on the principle of active triangulation, laser rays are expected to reflect on the object's surface before reaching back to the sensor. When projected on a rough surface, laser rays are partially absorbed or diffused in all directions, depriving the range sensor from the expected echo or creating false reflections that introduce errors on the range estimation. This phenomenon gets amplified as the external force that is applied on a soft object increases, given that the orientation of the local surface is significantly modified because it is no longer perpendicular to the laser beam

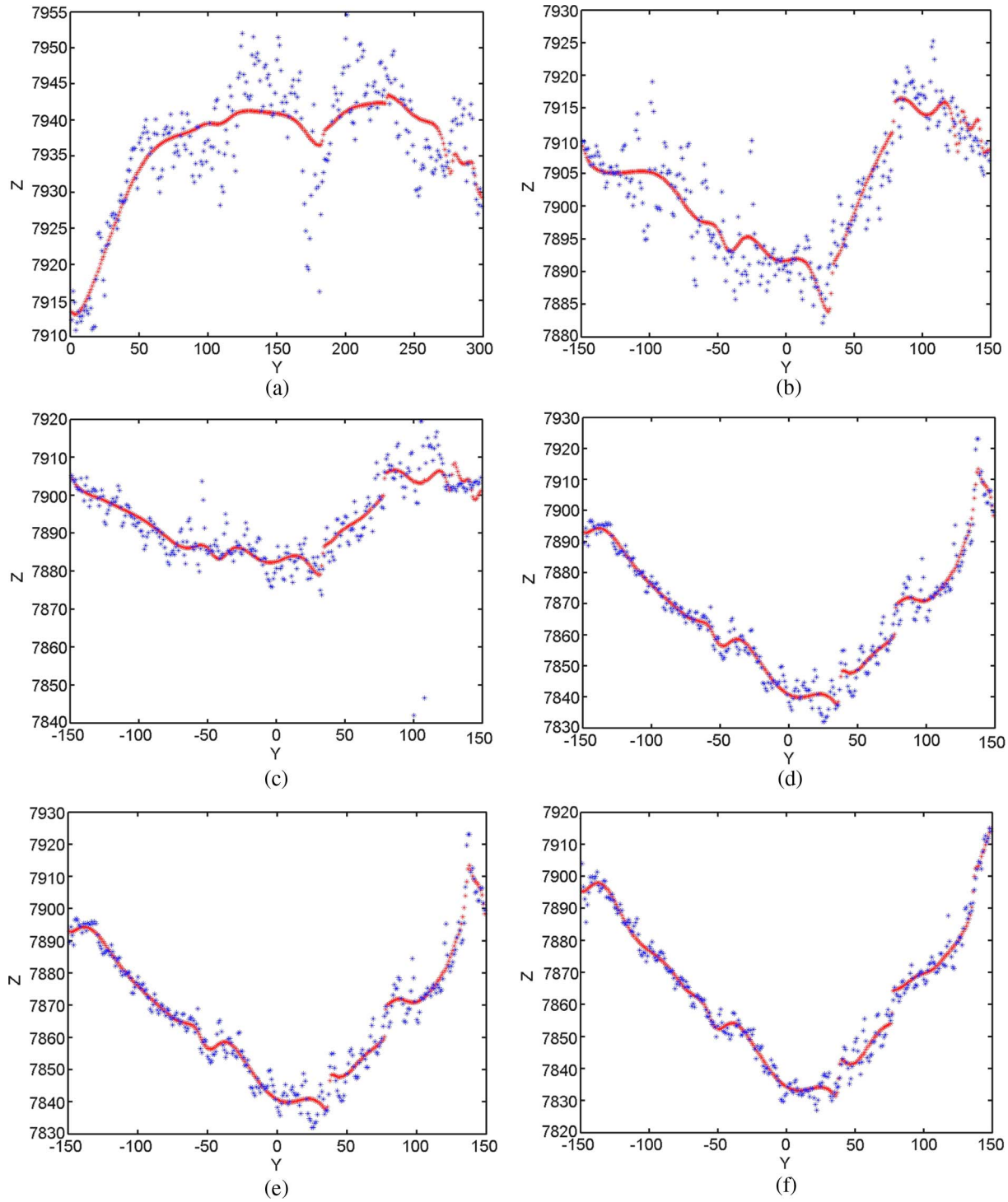

Fig. 15. Real and modeled deformation profiles for the cardboard under normal forces of (a) $F = 0.1$ N, (b) $F = 0.9$ N, (c) $F = 2.9$ N, (d) $F = 8$ N, (e) $F = 44.6$ N, and (f) $F = 46.7$ N.

propagation direction and, therefore, makes a gap appear around the probe's tip.

The deformation profiles are segmented to the regions of interest. Irrelevant information, such as the table that is depicted as straight lines around the value 8200 on the z-axis in Fig. 8, is removed, and only the part that contains the relevant deformation profile is provided in the training set.

The force magnitudes and the corresponding angles are provided as inputs to the network, and the normalized segmented deformation profiles are used as training samples. The networks that are associated with all materials are trained in five steps of 5000 epochs, each using the resilient propagation algorithm [24] that is implemented in the Matlab code, with the learning rate set to 0.1. The whole data set is used for training to provide enough samples. Training takes approximately 10 min on a Pentium IV 1.3-GHz machine with 512-MB memory. For the rubber, the sum-squared error reached during training is 3.7×10^{-3}, for the cardboard, it is 3.5×10^{-2},

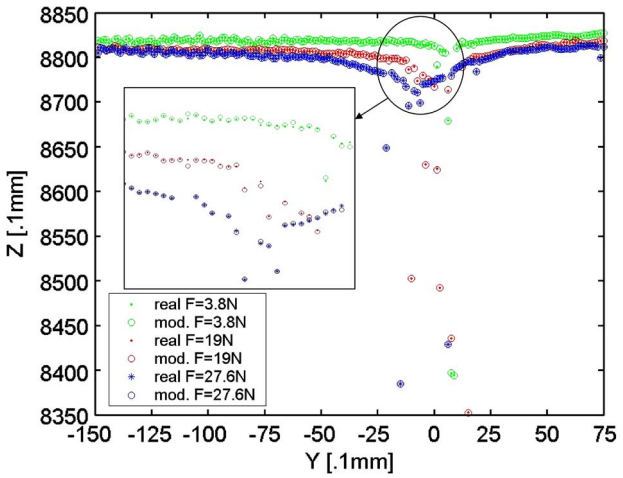

Fig. 16. Real and modeled deformation profiles and a detail of the deformation for the foam pillow under normal forces.

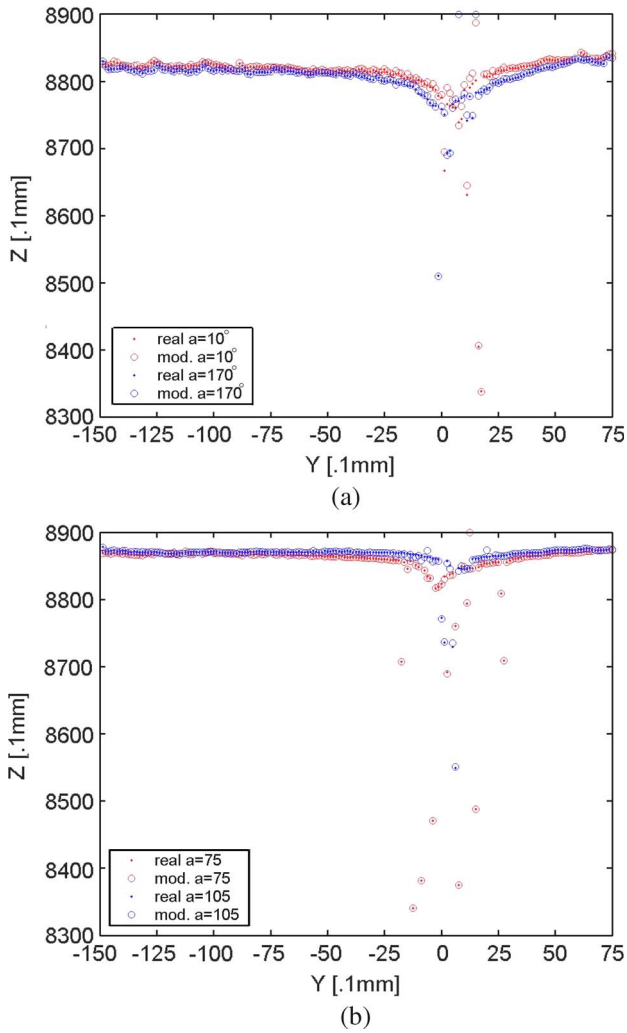

Fig. 17. Real and modeled deformation profiles for a foam pillow under forces applied at different angles. (a) $F = 16$ N, $a = 10°$; $F = 38$ N, $a = 170°$. (b) $F = 67$ N, $a = 75°$; $F = 5$ N, $a = 105°$.

whereas for the foam, it is 2.2×10^{-2}. As expected, the error is lower for the rubber, where the data are more compact and less noisy, whereas it remains slightly higher for the cardboard and even higher for the foam. However, in all cases, excellent convergence is achieved.

The accuracy of the model is validated by the results obtained while testing the networks for all three materials. First, the networks are tested with samples from the training data set. Fig. 13 shows the deformation characteristics for the rubber ball under three different force magnitudes that are applied at a normal angle on the surface of the object, whereas Fig. 14 shows a sample of the real and modeled segmented deformation profiles obtained for different forces that are applied at different angles on the same object. The real data are depicted by points, and the modeled data, as estimated by the neural network for the same inputs, are depicted by circles. The modeled data are very close to the real data, and as expected, the modeled deformation profiles for mirror angles (10° and 170°, and 25° and 155°) and for about the same force magnitude are roughly mirror profiles as well, as shown in Fig. 14.

Fig. 15 presents the real and modeled segmented deformation profiles for the cardboard material that is submitted to the subset of force magnitudes shown in Fig. 9. The data are noisier; however, the network is still able to cope with them and model the main shape of the deformation profile. Since there is no significant change in the deformation profile while probing the box at different angles, further results are not presented here. Fig. 16 shows real and modeled segmented deformation profiles that are obtained for the application of a normal force on the foam pillow, for the subset of forces in Fig. 10, whereas Fig. 17 shows the corresponding characteristics for the foam submitted to different forces that are applied at different angles. The network catches some of the noise in the curves but quite accurately models the deformation profiles. Even if it is less obvious in this case, the mirror angles still result in mirrored profiles.

All these experiments demonstrate the high potential of neural networks to extract the main features of highly nonlinear data sets while being fault tolerant and insensitive to noise that is inherently present in any real data. Sparse errors in the deformation profiles are successfully eliminated by the network. However, the neural model remains fully capable of capturing the peak of the deformation profile, even in areas where the profile does not contain numerous sampling points.

Moreover, our experimentation allowed the study of the generalization ability of the neural network model scheme. For this purpose, the network is tested for different forces and angles that were not part of the training set. Some results for the rubber material are depicted in Figs. 18 and 19. Fig. 18 shows the entire set as well as a detail of the real, modeled, and estimated deformation profiles for increasing forces that are applied at a constant angle (75°) on the rubber ball. The points denote the training data and the circles denote the modeled data, which consist of the estimation of the deformation when the network is presented with the training data, whereas the stars represent a deformation profile that is estimated by the network for a magnitude of force that was not included in the training set. The network correctly places the estimated profiles where expected. For example, the estimated profile for a force of 68 N is placed in between the real measured profiles of 64.4

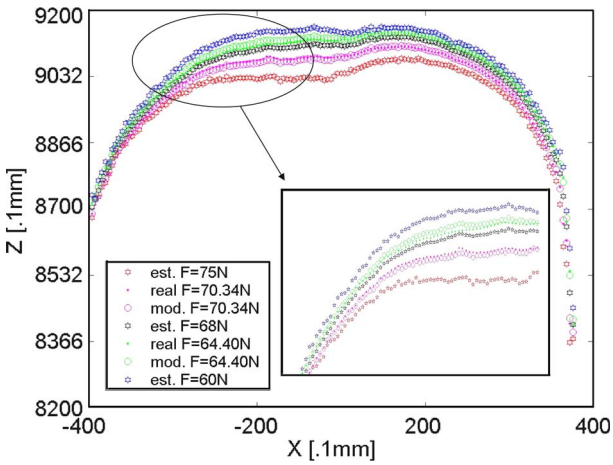

Fig. 18. Real, modeled, and estimated deformation profiles and detail of the estimated deformation for a rubber ball under increasing forces applied at a 75° angle.

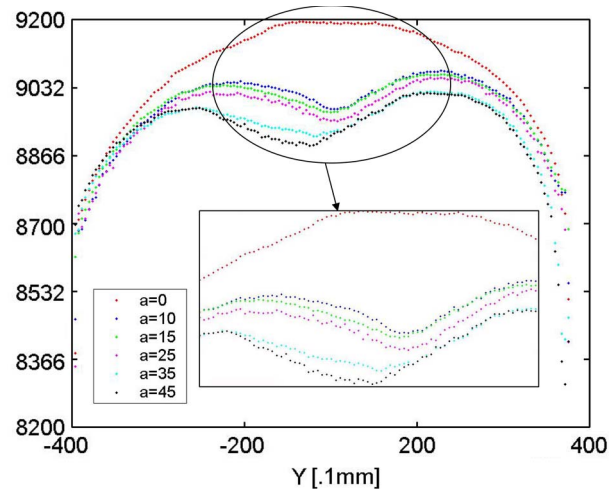

Fig. 19. Estimated deformation profiles and detail of the estimated deformation profiles using the neural network for the rubber ball for the same force $F = 40$ N applied at different angles.

and 70.34 N, whereas the cavity in the profile, corresponding to the same angle used, is slightly moving to the right, as expected.

Another test reveals the ability of the network to estimate deformation profiles for a constant force applied at different angles that was not part of the initial training set. Fig. 19 depicts the deformation profiles that are estimated for a constant force of 40 N and increasing angles between 0° and 45°. The position of the profiles in relation to each other and to the cavity of each profile corresponds to what one would expect it to be. As the force is the same, but the angle increases (valid for angles under 90°), the cavity becomes slightly deeper and shifted toward the left. The network, therefore, generalizes well, being able to provide good estimates for both angles and forces that are not part of the training set.

VI. Conclusion and Future Work

This investigation demonstrates that the benefit of using neural networks to model deformable objects is threefold. First, neural networks provide continuous output behavior, being able to provide the necessary nonlinear interpolation for estimates of data that were not part of the training set. When compared with most of the work found in the literature, where *a priori* knowledge about the characteristics of the material is assumed available, this paper proposes a robust approach for modeling force/deformation relationships from realistic experimental data with noisy and incomplete measurements, the latter being exemplified here by missing values for some of the points along the scanline.

Second, the use of a neural network modeling scheme avoids the problem, which is complicated and frequently impossible to solve, of recuperating explicit elastic parameters, particularly for highly nonlinear elastic materials. Last, neural networks provide an accurate and fast response without requiring the high computation times that are associated with the solution of mathematical models of deformable objects.

Combined with the neural gas network that significantly reduces the number of sample points that are needed to accurately represent a 3-D deformable object, the proposed approach to model elasticity proves to be an efficient way to measure, construct, and represent elastic deformable objects since performing raster tactile probing on large surfaces would be prohibitive.

As future work, we plan to enhance the proposed approach by performing scans of the deformation profiles over different directions. This will enable the application to obtain a 3-D deformation profile model for each interaction point.

References

[1] D. Aulignac, C. Laugier, and M. C. Cavusoglu, "Towards a realistic echographic simulator with force feedback," in *Proc. IEEE/RSJ Int. Conf. Intell. Robots Syst.*, Kyongju, Korea, 1999, pp. 727–732.

[2] C. Monserrat, U. Meier, M. Alcañiz, F. Chinesta, and M. C. Juan, "A new approach for the real-time simulation of tissue deformations in surgery simulation," *Comput. Methods Programs Biomed.*, vol. 64, no. 2, pp. 77–85, Feb. 2001.

[3] D. K. Pai, K. van den Doel, D. L. James, J. Lang, J. E. Lloyd, J. L. Richmond, and S. H. Yau, "Scanning physical interaction behavior of 3D objects," in *Proc. SIGGRAPH, 28th Annu. Conf. Comput. Graph. Interactive Tech.*, Los Angeles, CA, Aug. 2001, pp. 87–96.

[4] H. T. Tanaka, K. Kushihama, and N. Ueda, "A vision-based haptic exploration," in *Proc. IEEE Int. Conf. Robot. Autom.*, Taipei, Taiwan, R.O.C., 2003, pp. 3441–3448.

[5] K. K. Tho, S. Swaddiwudhipong, Z. S. Liu, and J. Hua, "Artificial neural network model for material characterization by indentation," *Model. Simul. Mater. Sci. Eng.*, vol. 12, no. 5, pp. 1055–1062, Sep. 2004.

[6] N. Ueda, S. Hirai, and H. T. Tanaka, "Extracting rheological properties of deformable objects with haptic vision," in *Proc. IEEE Int. Conf. Robot. Autom.*, Barcelona, Spain, Apr. 2004, pp. 3902–3907.

[7] A. M. Okamura, J. T. Dennerlein, and R. D. Howe, "Vibration feedback models for virtual environments," in *Proc. IEEE Int. Conf. Robot. Autom.*, Leuven, Belgium, May 1998, pp. 2485–2490.

[8] Y. Zhu, T. J. Hall, and J. Jiang, "A finite-element approach for young's modulus reconstruction," *IEEE Trans. Med. Imag.*, vol. 22, no. 7, pp. 890–901, Jul. 2003.

[9] J. Li, M. Wan, M. Qian, and J. Cheng, "Elasticity measurement of soft tissue using shear acoustic wave and real-time movement estimating based on PCA neural network," in *Proc. Int. Conf. IEEE Eng. Med. Biol. Soc.*, Hong Kong, Oct. 1998, vol. 3, pp. 1395–1396.

[10] M. A. Greminger and B. J. Nelson, "Modeling elastic objects with neural networks for vision-based force measurement," in *Proc. Int. Conf. Intell. Robots Syst.*, Las Vegas, NV, Oct. 2003, pp. 1278–1283.

[11] K. Kamiyama, H. Kajimoto, M. Inami, N. Kawakami, and S. Tachi, "A vision-based tactile sensor," in *Proc. Int. Conf. Artif. Reality Telexistence*, Tokyo, Japan, 2001, pp. 127–134.

[12] K. Kamiyama, H. Kajimoto, N. Kawakami, and S. Tachi, "Evaluation of a vision-based tactile sensor," in *Proc. IEEE Int. Conf. Robot. Autom.*, Barcelona, Spain, Apr. 2004, vol. 2, pp. 1542–1547.
[13] V. Vuskovic, M. Krauer, G. Szekely, and M. Reidy, "Realistic force feedback for virtual reality based diagnostic surgery simulators," in *Proc. IEEE Int. Conf. Robot. Autom.*, San Francisco, CA, Apr. 2000, pp. 1592–1598.
[14] X. Wang, G. K. Ananthasuresh, and J. P. Ostrowski, "Vision-based sensing of forces in elastic objects," *Sens. Actuators A, Phys.*, vol. 94, no. 3, pp. 146–156, Nov. 2001.
[15] N. J. Ferrier and R. W. Brockett, "Reconstructing the shape of a deformable membrane from image data," *Int. J. Robot. Res.*, vol. 19, no. 9, pp. 795–816, 2000.
[16] D. Hristu, N. Ferrier, and R. W. Brockett, "The performance of a deformable-membrane tactile sensor: Basic results on geometrically-defined tasks," in *Proc. IEEE Int. Conf. Robot. Autom.*, San Francisco, CA, Apr. 2000, vol. 1, pp. 508–513.
[17] A.-M. Cretu and E. M. Petriu, "Neural-network-based adaptive sampling of three-dimensional-object surface elastic properties," *IEEE Trans. Instrum. Meas.*, vol. 55, no. 2, pp. 483–492, Apr. 2006.
[18] A.-M. Cretu, E. M. Petriu, and P. Payeur, "Neural network mapping and clustering of elastic behavior from tactile and range imaging for virtualized reality applications," in *Proc. IEEE Int. Workshop Imag. Syst. Techn.*, Minori, Italy, 2006, pp. 17–22.
[19] A.-M. Cretu, J. Lang, and E. M. Petriu, "A composite neural-gas Elman network that captures real-world elastic behavior of 3D objects," in *Proc. IEEE Instrum. Meas. Technol. Conf.*, Sorrento, Italy, 2006, pp. 1063–1067.
[20] *Installation and Operations Manual for Stand-Alone F/T Sensor Systems*, ATI Ind. Autom. Inc., Garner, NC, 1997.
[21] *Jupiter 3-D Laser Vision Camera Installation and Operation Manual*, Servo-Robot Inc., St. Bruno, QC, Canada, 1996.
[22] J. R. Jang, C. T. Sun, and E. Mizutani, *Neuro-Fuzzy and Soft Computing. A Computational Approach to Learning and Machine Intelligence*. Englewood Cliffs, NJ: Prentice-Hall, 1997.
[23] J. N. Noyes, "Neural network training," in *Handbook of Neural Computation*, E. Fiesler and R. Beale, Eds. London, U.K.: Oxford Univ. Press, 1997.
[24] M. Riedmiller and H. Braun, "A direct adaptive method for fast backpropagation learning: The RPROP algorithm," in *Proc. IEEE Int. Conf. Neural Netw.*, San Francisco, CA, 1993, pp. 586–591.

Ana-Maria Cretu (S'04) received the M.S. degree from the School of Information Technology and Engineering, University of Ottawa, Ottawa, ON, Canada, where she is currently working toward the Ph.D. degree.

Her research interests include neural networks, tactile sensing, 3-D object modeling, and multisensor data fusion.

Ms. Cretu is a Student Member of the IEEE Instrumentation and Measurement and IEEE Computational Intelligence Societies.

Pierre Payeur (S'90–M'98) received the Ph.D. degree in electrical engineering from the Université Laval, Quebec City, QC, Canada, in 1999.

He is a Founding Member of the Vision, Imaging, Video, and Autonomous Systems Research Laboratory and a member of the Sensing and Modeling Research Laboratory. In 1998, he joined the University of Ottawa, Ottawa, ON, Canada, where he is currently an Associate Professor with School of Information Technology and Engineering. His current research interests include 3-D imaging and modeling, range data processing, robot guidance, teleoperation, motion capture, and integration of computer vision in autonomous systems.

Dr. Payeur is a member of the IEEE Robotics and Automation Society, the IEEE Instrumentation and Measurement Society, and the Ordre des Ingénieurs du Québec.

Emil M. Petriu (M'86–SM'88–F'01) received the Dipl.Eng. and Dr.Eng. degrees from the Polytechnic Institute of Timisoara, Timisoara, Romania, in 1969 and 1978, respectively.

Since 1985, he has been a member of the faculty of the University of Ottawa, Ottawa, ON, Canada, where he is currently a Professor and the University Research Chair with School of Information Technology and Engineering. Since 2005, he has been serving as the Chief Scientific Officer of XYZ RGB, Inc., which is a 3-D imaging company in Ottawa. His research interests include robot sensing and perception, interactive virtual environments, human–computer symbiosis, soft computing, and digital integrated circuit testing. During his career, he has published more than 280 technical papers, authored two books, and edited two other books. He is the holder of two patents.

Dr. Petriu is a Fellow of the Canadian Academy of Engineering and of the Engineering Institute of Canada. He was a corecipient of the IEEE's Donald G. Fink Prize Paper Award and the recipient of the IEEE Instrumentation and Measurement Society Award in 2003. He is currently serving as the Chair of TC-15 Virtual Systems and the Cochair of TC-28 Instrumentation and Measurement for Robotics and Automation TC-30 Security and Contraband Detection of the IEEE Instrumentation and Measurement Society. He has been actively involved in the organization of many international conferences, symposia, and workshops. He was the General Chair of the IEEE Instrumentation and Measurement Technology Conference (IMTC), Ottawa, in May 2005 and the Program Chair of IMTC, Ottawa, in 1997, IMTC, St. Paul, MN, in 1998, IMTC, Anchorage, AK, in 2002, and I^{2}MTC, Victoria, BC, Canada, in 2008. He is an Associate Editor of the IEEE TRANSACTIONS ON INSTRUMENTATION AND MEASUREMENT and a member of the editorial board of the *IEEE Instrumentation and Measurement Magazine*.